A compact four-element electromagnetic band gap and slots-inspired ultra-wideband multiple-input-multiple-output antenna with quad-band rejection characteristics

Ranjana Kumari[1,2], Vinay Kumar Tomar[1]
[1]Department of Electronics and Communication Engineering, GLA University, Mathura, Uttar Pradesh, India
[2]Department of Electronics and Communication Engineering, Galgotias College of Engineering and Technology, Greater Noida, Uttar Pradesh, India

Corresponding author: Vinay Kumar Tomar (e-mail: vinay.tomar@gla.ac.in).

ABSTRACT In this research, a four-element multiple-input-multiple-output (MIMO) antenna with ultra-wideband (UWB) operating range and quad-notch characteristics at WLAN (4.7-5.9 GHz), X-band uplink and downlink satellite systems (6.6-8.1 GHz), X-band NATO type-2 spectrum (8.6-10.96 GHz), and Ku-band fixed satellite services (FSS) and direct broadcast satellite (DBS) services (11.6-12.9 GHz) is designed on the FR-4 substrate of dimensions of $0.28\lambda_0 \times 0.32\lambda_0 \times 0.01\lambda_0$ (28 mm × 36 mm × 1 mm). In order to attain inter-element isolation of more than 20 dB, a pair of inverse-L stubs is introduced in the common ground plane of the proposed antenna. Additionally, good radiation characteristics with a maximum gain of 5.6 dBi and diversity parameters have been analyzed with envelope correlation coefficient (ECC < 0.001), diversity gain (DG > 9.5 dB), mean effective gain (MEG ≤ -3 dB), and total active reflection coefficient (TARC < -10 dB). The measured and simulated results of the proposed MIMO antenna, operating from 3.1 to 15.2 GHz, validate that it is a good choice for wireless communication applications.

INDEX TERMS EBG, MIMO, quad-port, ultra-wideband, WLAN, X-band

I. INTRODUCTION

Due to low power transmission and high data rate features, the ultra-wideband (UWB) spectrum with 3.1 -10.6 GHz has been ofently used for short-range communication applications [1]-[2]. To accomplish the prerequisite of UWB applications, challenges of antenna design pertain to compact size, impedance matching, and omnidirectional radiation patterns. A single antenna faces multipath fading and signal interference, which is the main cause of degrading the performance of wireless network links. To improve the performance, UWB multiple-input-multiple-output (MIMO) technology is utilized to suppress multipath fading and improve data transmission rate [3]-[5]. However, UWB MIMO antennas exhibit significant correlation among radiators due to the narrow spacing of antenna elements [6]. Therefore, various isolation techniques have been reported to achieve a low correlation coefficient among radiating elements.

In [7]-[10], different shapes of slots or stubs are loaded between radiating elements for isolation improvement. However, communication systems operating at WLAN (5.15-5.85 GHz), satellite communication bands (7.25-7.75 GHz), X-band (8-12 GHz), and Ku-band (11.75-12.5 GHz) interfere with the existing UWB spectrum. Therefore, UWB MIMO antennas with band rejection capability are required to reject such frequency bands [11]. Recently, a dual-port MIMO antenna has been designed to reject single-band interference (WiMAX, WLAN, X-band) in [12]-[14], and MIMO antenna designs with two-notch rejection capability are discussed in [15]-[18]. Apart from the quarter-wavelength and half-wavelength slots to reject the narrowband interference, electromagnetic band gap (EBG) structures are also employed for band rejection in MIMO antennas in [19]-[20]. In [21], a two-element UWB antenna with triple-notched bands rejection at 4.56 GHz, 7.25 GHz, and 9.08 GHz is designed, and by placing them in an orthogonal arrangement, reduction in mutual coupling is achieved. In [22], three slots along with mushroom-shaped EBG are loaded in the radiating patches for quad-band suppression in UWB spectrum. Further, to enhance the data rate and channel capacity, a four-port MIMO antenna with a small footprint of 48 mm × 34 mm and isolation >22 dB is achieved by inserting a neutralization line in [23]. Similarly, four-port MIMO antennas with good isolation between the radiating elements are proposed with single-notch band suppression in [24]-[25] and dual-band rejection capability

in [26]-[27]. Recently, authors in [28]-[30] have presented compact four-port MIMO antennas with triple-notch band characteristics. In [28]-[30], MIMO antennas are presented with different shapes of slots and EBG structures to achieve notch bands suppression.

As per the literature, band-notched UWB MIMO antenna designs faces challenges with isolation techniques impacting compactness and design simplicity. For frequencies above 11 GHz (covering the X-band and Ku-band, including fixed satellite services (FSS) and direct broadcast satellite (DBS)), most of the existing MIMO antenna designs fail to effectively reject interference from the Ku2-band while maintaining high isolation and stable gain. However, the size of existing four-port MIMO antennas is relatively large. Four-port MIMO antenna with quad-band rejection characteristics for X-band NATO type-2 spectrum and Ku-band (FSS and DBS) frequency range (3.1 to 15.2 GHz) is essential for UWB applications and still, it is a big challenge.

The main features of the presented antenna are: (i) The profile of tapered fed four-port UWB MIMO antenna with physical dimensions of $00.28\lambda_0 \times 0.32\lambda_0 \times 0.01\lambda_0$ (28 mm × 36 mm × 1 mm) is small with peak gain of 5.6 dBi, demonstrating superior performance compared to existing MIMO antennas, (ii) By inserting a pair of L slots on the radiator and a half-wavelength ($\lambda_g/2$) U-shaped slot, and loading of EBG structures on the feed line to achieve quad notch bands (4.7-5.9 GHz, 6.6-8.1 GHz, 8.6-10.9 GHz, and 11.6-12.9 GHz) with high rejection and stable gain characteristics, (iii) Inserting the pair of inverse-L stubs in the common ground ensures that the isolation >20, while maintaining satisfactory diversity characteristics throughout the spectrum (3.1-15.2 GHz), (iv) Connected ground planes of the antenna elements ensures the common reference voltage in the ground surface of the MIMO antenna.

This article is divided into sections: Design and analysis of four-port MIMO antenna are discussed in section II. Simulated and measured results of quad-port MIMO antenna, in terms of S-parameters, far-field characteristics, diversity performance analysis, and comparison of the proposed MIMO antenna with existing antennas in section III. And, the conclusion is stated in section IV.

II. FOUR PORT MIMO ANTENNA DESIGN WITH QUAD-BAND REJECTION CHARACTERISTICS

A. EVOLUTION OF TWO-PORT UWB MIMO ANTENNA WITH NOTCH BANDS

The progression of the dual-port MIMO antenna with quad rejection band characteristics is depicted in Fig. 1. The designed antenna consists of two key-shaped radiating elements printed on the low-cost FR-4 substrate of relative permittivity of $\varepsilon_r = 4.4$ and height of $t = 1$ mm. The physical size of the substrate is 28 mm × 18 mm × 1 mm. In Fig. 1(a), two rectangular-shaped monopole radiators are designed to achieve UWB impedance bandwidth (3.1-15 GHz). The lower resonant frequency of Ant. 1 is computed through equation (1).

$$f_{r0} = \frac{7.2}{\{(W_1+b+g)\times k\}} \quad (1)$$

The lower resonant frequency is directly dependent on parameters W_1, L_1, b, g, and $\varepsilon_{eff} = (\varepsilon_r + 1)/2$.
Here, the width of the patch is W_1 and the length of the patch is L_1. The space between lower edge of the patch and the ground plane is g and $b = L_1/2\pi$ [22].
Due to gap g (mm) between patch and ground, Ant. 1 is not providing proper impedance matching throughout UWB spectrum. The simulated results of Ant. 1 is shown in Fig. 2. Due to poor impedance matching in Ant. 1, the rectangular-shaped radiator is modified with two arcs with radius R to achieve the UWB (3.1-15 GHz) in Ant. 2. The UWB of Ant. 2 makes it inclined to interference from other nearby narrowband systems. To reject interference from nearby narrowband systems, the next step is to add band reject filters to existing antenna to reject interference band.

The L-slot [22] and EBG structures [30] function like a band stop filter by capturing and storing all the input energy at their resonant frequency. This approach is quite similar to the design of a band-stop filter. To attain quad-notch characteristics with high isolation in spectrum, alterations in antennas (Ant. 2-Ant. 7) are depicted in Fig. 1(b)-(g), each design has been simulated using CST Microwave Studio software. To maintain the isolation >20 dB, a pair of inverted-L stubs are inserted in the ground plane, with optimized distance $L_e = 11$ mm, among elements in each stage (Ant. 1-Ant. 7). The physical dimensions of all stages are described in Table I.

Therefore, to realize the quadruple band-notch characteristics, firstly an inverted open-ended L-slot is etched out from Ant. 3 as illustrated in Fig. 1(c). Consequently, Ant. 3 is competent in rejecting an interfering frequency band (4.7-5.8 GHz) as illustrated in Fig. 2. Similarly, to obtain dual-notch characteristics, one more L-shaped slot is created in the radiating element of Ant. 4 as illustrated in Fig. 1(d). Hence, Ant. 4 stage is competent in rejecting two different interfering frequency bands (4.7-5.9 GHz and 6.3-7.8 GHz). Furthermore, a U-shaped slot is etched out from the tapered feed line area to design the Ant. 5 as depicted in Fig. 1(e). The U-shaped slot in Ant. 5 is responsible for removing the third frequency band interference (9.6-11.6 GHz). However, Ant. 5 is not able to produce third notch band for NATO type-2 (8.6 to 10.63 GHz).

Moreover, introducing one more notched band for 11.6-12.9 GHz (Ku-band, FSS and DBS) without changing dimensions of the previous stage, a pair of circle-shaped EBG structures with radius $R_2 = 1.5$ mm and vias of radius $R_1 = 0.5$ mm are introduced adjacent to the tapered feed line in Fig. 1(f). Thus, Ant. 6 with the combination of EBG structures with slots is designed to attain quad rejection band characteristics. As per the observation, Ant. 6 fails to produce Ku=band (FSS and DBS) interference and shifts the third notch towards the right side. To optimize Ku-band for

(FSS and DBS) 11.6-12.9 GHz along with other notches, circle-shaped EBG structures are modified into water drop-shaped EBG structures to form the Ant. 7 in Fig. 1(g). Finally, three optimized slots with EBG composition are implanted to reject the interference of WLAN (4.7-5.9 GHz), satellite communication downlink (6.6-8.1 GHz), X-band NATO type-2 spectrum (8.6-10.9 GHz), and Ku-band (11.6-12.9 GHz).

To optimize bandwidth of first, second, and third notches, effective length of each slot (L_{slot1}, L_{slot2}, and U_{slot3}) can be easily determined by using equations (2)-(5) in [22], [26], and [28], where f_{n_slot1}, f_{n_slot2}, and f_{n_slot3} are resonant frequencies of notch bands.

$$L_{slot1} = S_1 + S_2 = \frac{c}{4f_{n\_slot1}\sqrt{\varepsilon_{eff}}} \quad (2)$$

$$L_{slot2} = S_3 + S_4 = \frac{c}{4f_{n\_slot2}\sqrt{\varepsilon_{eff}}} \quad (3)$$

$$U_{slot3} = (2 * S_5) + S_6 + (S_6 - A_3) = \frac{c}{2f_{n\_slot3}\sqrt{\varepsilon_{eff}}} \quad (4)$$

$$\varepsilon_{eff} = \frac{\varepsilon_r + 1}{2} \quad (5)$$

To optimize the prediction of the fourth notch for Ku-band (FSS and DBS) by water drop-shaped EBG structure, the resonant frequency (f_{r_EBG}) of the fourth notch is computed through equation (6). The values of L, C_1, and C_2 are calculated using equations (7)-(9). In equation (7), capacitance C_1 represents the coupling capacitance between the feed-line and the edge of the EBG. Meanwhile, capacitance C_2 is attributed to the voltage gradient between the water drop-shaped EBG patch and the ground in equation (8). The inductance L is generated by the current flowing through the via in equation (9).

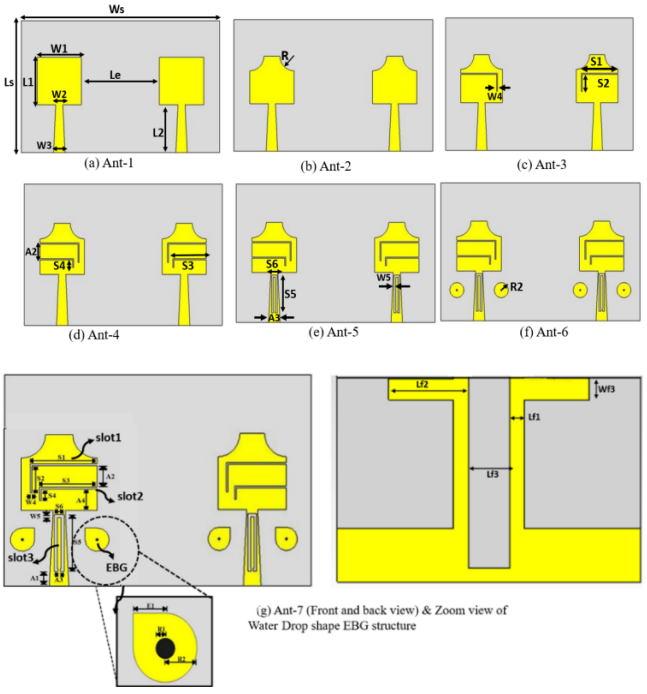

FIGURE 1. Design progression of the MIMO antenna (a) Ant-1, (b) Ant-2, (c) Ant-3, (d) Ant-4, (e) Ant-5, (f) Ant-6, (g) Ant-7.

$$f_{r\_EBG} = \frac{1}{2\pi\sqrt{L(C_1 + C_2)}} \quad (6)$$

$$C_1 = \frac{E_1\varepsilon_0(1+\varepsilon_r)}{\pi} cosh^{-1}\left(\frac{E_1+S}{S}\right) \quad (7)$$

where E_1 is the sub-length of the water drop-shaped EBG structure and the S gap between the EBG and the feed line. The values of E_1 and S are illustrated in Table I.

$$C_2 = \frac{\varepsilon_0\varepsilon_r A_{EBG}}{t} \quad (8)$$

$$L = \frac{\mu_0 * t}{2\pi} * \left(\frac{2 * t}{R1/2}\right) \quad (9)$$

where A_{EBG} is the area of the water drop-shaped EBG structure and R_1 is the diameter of the via.

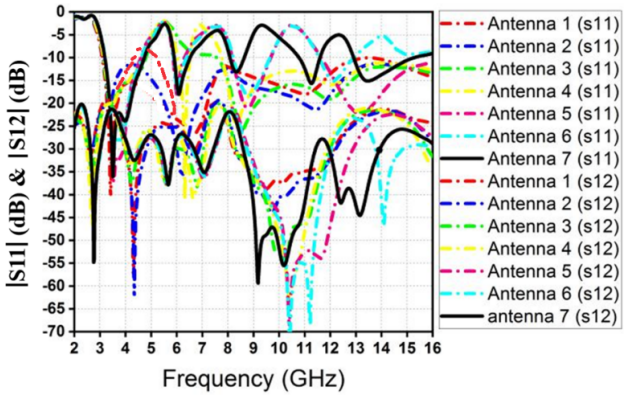

FIGURE 2. Simulated S-parameters of two-port MIMO antenna design.

TABLE I. Dimensions of the proposed MIMO antenna.

L	S_1	W	L_1	S_2	W_1	L_2
36	5.5	28	6.5	2.35	6.25	6.5
W_3	L_{f2}	S_5	W_4	L_{f3}	S_6	W_5
1.6	6	4.4	0.15	3.8	0.8	0.25
A_2	W_{f2}	R_2	A_3	W_{f3}	E_1	A_4
1.85	1.25	1.5	0.2	2	1	1.25
W_2	L_{f1}	S_4	E_2	A_1	W_{f1}	R_1
1	1.35	1	1.5	0.85	5	0.5
W_{f2}	R_2	S	S_3	R	P	
1.25	1.5	1.2	4.75	2	2.25	

B.PARAMETRIC ANALYSIS AND SURFACE CURRENT DISTRIBUTION

In this section, the impact of slot lengths (S_2 (mm), S_4 (mm), and S_5 (mm)) on impedance bandwidth is illustrated in Figs. 3(a)-(d). The S_2, S_4, and S_5 are sub lengths of L_{slot1}, L_{slot2}, and U_{slot3}, respectively. The total length of L_{slot1} varies when sub-length S_2 alters from 1.35 to 3.35 mm. The resonant frequency shifts from 6.5 to 5.1 GHz, and the first notch is obtained at S_2 = 2.35 mm, which eventually slightly hinders the required band as depicted in Fig. 3(a). The length of L_{slot1} = 7.85 mm is the same as the calculated length by equation (2).

Similarly, the variation of S_4 is simulated to reject interference from 6.58-8.1 GHz. The parametric results for S_4 = 0 to 1.5 mm are illustrated in Fig. 3(b). As per observation, the third and fourth notch bands are completely diminished at S_4 = 0 mm. When S_4 (mm) increases from 0 to 1 mm, the optimized notch bands are obtained. Furthermore, when the sub-length of the slot (S_4 = 1.5 mm) changes, the center frequency of the notch band is shifted from 7.5 to 7 GHz, shifting the notched band spectrum.

The variations of S_5 is simulated to remove the interference from the 8.9-10.6 GHz band, and the parametric results of length S_5 are illustrated 3.4 to 5.5 mm as shown in Fig. 3(c). As per observation, the third notch band is completely diminished at 3.4 mm without affecting the first and second notchs. Therefore, a length of 3.4 mm is not enough to provide an optimized notch frequency band (8.6-10.96 GHz). Finally, the optimized results are obtained at 4.4 mm as slight changes were affecting the band shift towards left and right and even hindering the previous bands as well at S_5 = 5.4 mm.

The water drop-shaped EBG design is placed near to antenna feeding line to reject the 11.6-12.9 GHz band. The distance of the EBG structure from patch lower edge (E_2) critically impacted to desired rejection band. Therefore, to achieve the desired notch band, parametric analysis of simulated results have been analyzed at different values of E_2 as illustrated in Fig. 3(d). At E_2 = 0.5 mm, the notch band has shifted to the left without affecting the previous band, and at a distance of 2 mm, a fourth notch is completely diminished. When the E_2 length is reduced to 1.5 mm, the optimized results of the notch band are achieved with bandwidth of 11.6-12.9 GHz for Ku-band FSS and DBS services.

To validate the effect of slots and EBG structure on the notch rejection capability, current distribution(A/m)

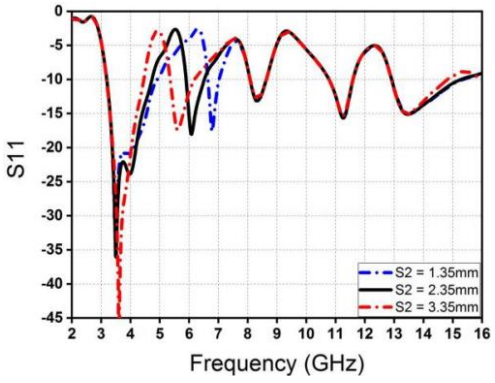

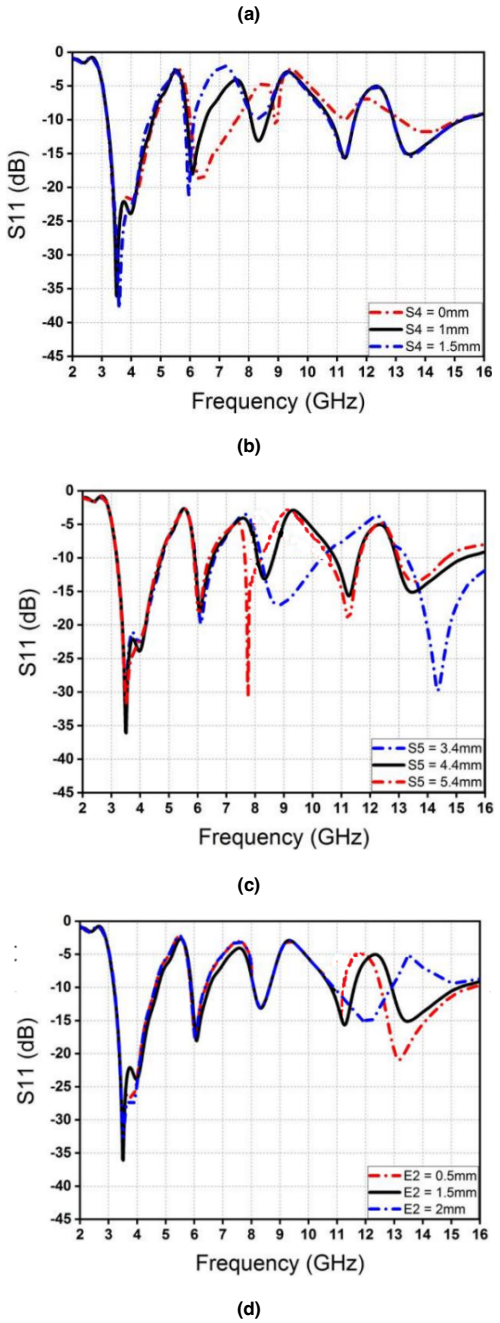

FIGURE 3. Parametric analysis of the proposed antenna (a) S_2 (mm) of L_{slot1}, (b) S_4 (mm) of L_{slot2}, (c) S_5 (mm) of U_{slot3}, (d) E_2 (mm) of EBG_{length}.

at notch resonant frequencies are depicted in Figs. 4(a)-(d) with port 1 excited.

The surface current distribution at 5.5 GHz is depicted in Fig. 4(a). The concentration of surface current (A/m^2) is observed high near the L_{slot1}, capturing and storing all the input energy at their resonant frequency, providing the rejection at the WLAN band. Therefore, the individual band-rejection structure behaves like a non-radiator at the related band-rejection recurrence. Fig. 4(b) describes the surface current density at 7.5 GHz for second notched resonant

frequency. As per observation, current density is more dominant in the L_{slot2} rather than elsewhere.

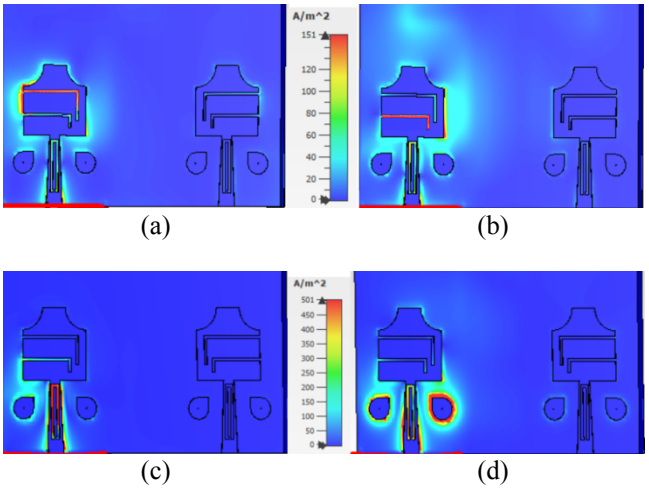

FIGURE 4. Surface Current distribution at (a) 5.5 GHz, (b)7.5 GHz, (c) 9.3 GHz, (d) 12.3 GHz.

Further, surface current (A/m^2) at 9.3 GHz is large in the U_{slot3} as compared to other areas in the proposed antenna as depicted in Fig. 4(c). The current surface density (A/m^2) at 12.3 GHz is more dominant on water drop-shaped EBG structures, rather than slots as illustrated in Fig. 4(d).

C. IMPEDANCE CHARACTERISTICS AND EQUIVALENT CIRCUIT OF TWO-PORT MIMO ANTENNA

In the previous section, the proposed antenna is analyzed in terms of S-parameters. But to better understand the mechanism of the proposed antenna (with filter), simulated impedance characteristics curve and its equivalent circuit are illustrated in Figs. 5(a)-(b). As per observation in Fig. 5(a), simulated impedance characteristics show high mismatch of impedance in notched bands, which shows series, parallel, or both series-parallel combination of the resonance circuit. For WLAN (4.7-5.9 GHz), the value of real impedance is 10.8 Ω at 5.46 GHz, with imaginary value varying from negative to positive resulting in a series resonant circuit as illustrated in in Fig. 5(b). For X-band uplink and downlink satellite system (6.6-8.1 GHz), X-band NATO type-2 spectrum (8.6-10.9 GHz), and Ku-band (FSS and DBS) (11.6-12.9 GHz), GHz), and Ku-band (FSS and DBS) (11.6-12.9 GHz), the real values of impedance are high and imaginary values varying from positive to negative resulting resulting in parallel *RLC* circuits. The combined equivalent values of series and parallel *RLC* circuits for quad-notch analysis are shown in Fig. 5(b) with load.

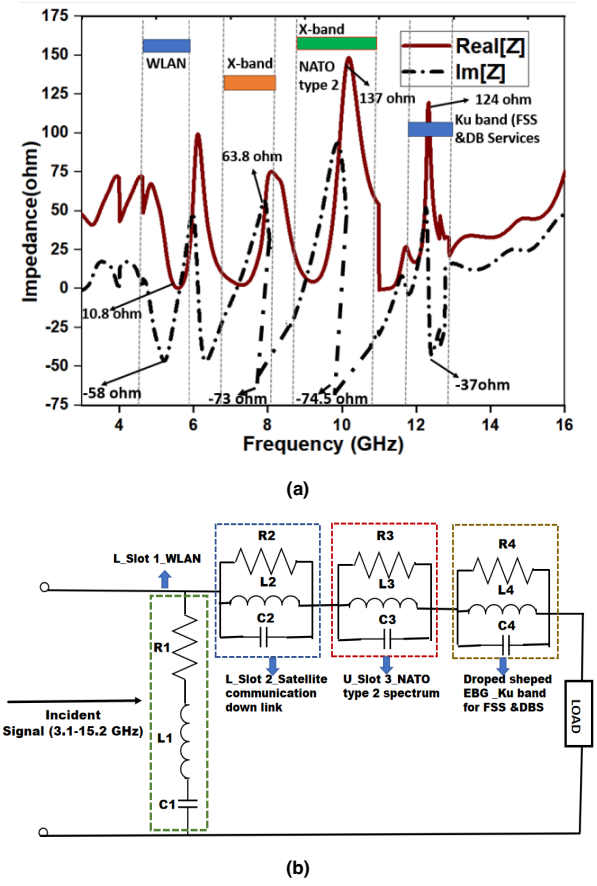

FIGURE 5. (a) Impedance characteristics of the proposed antenna with notches, (b) Equivalent circuit for with notches.

D. IMPLEMENTATION OF FOUR-ELEMENT UWB MIMO ANTENNA WITH REJECTION BANDS

After optimizing the dual-port MIMO antenna with rejection characteristics, it is extended into a quad-port MIMO antenna. The simulations of four-port MIMO antenna with quad-band notch characteristics are performed in CST Microwave Studio software. The layout of the proposed MIMO antenna with physical dimensions 28 mm × 36 mm × 1 mm is shown in Fig. 6. The front and back views of the proposed MIMO antenna design are illustrated in Figs. 6(a)-(b). To clear the physical dimensions, enlarged views of the radiator and EBG structure are illustrated in Figs. 6(c)-(d). All geometrical dimensions of the designed antenna with quad-port are depicted in Table I. The front and back views of the fabricated MIMO antenna are illustrated in Fig. 7. The result and discussion section discusses the simulated and measured results of the proposed MIMO antenna.

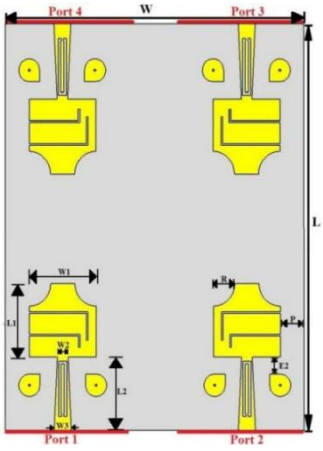

(a)

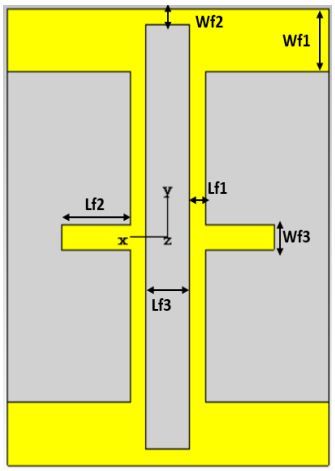

(b)

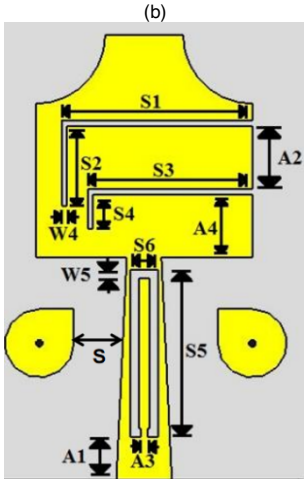

(c)

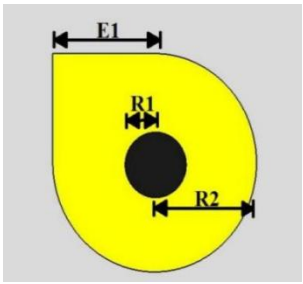

(d)

FIGURE 6. (a) Front view, (b) Back view of reported MIMO antenna, (c) Zoomed view of the radiator, (d) EBG structure.

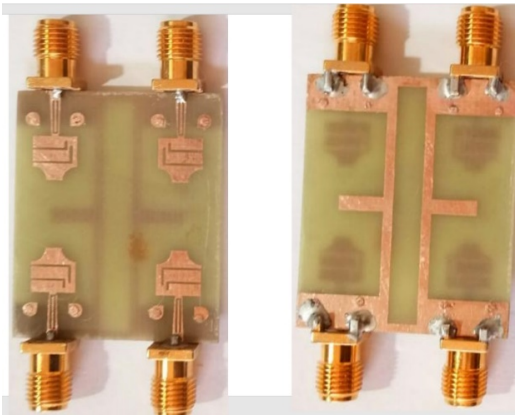

(a) (b)

FIGURE 7. Fabricated MIMO antenna (a) Front view, (b) Back view.

III. RESULTS AND DISCUSSION

In this section, the simulated and measured results have been discussed. Scattering parameters of the fabricated prototype are measured by vector network analyzer(VNA) and radiation pattern and gain are measured in the anechoic chamber. The simulated and measured results of proposed MIMO antenna are also compared in this section.

A. SCATTERING PARAMETERS

In Fig. 8, the fabricated MIMO antenna is measured with VNA for S-parameters. The simulated and measured S-parameters are compared in Figs. 9(a)-(c). It is clear from Fig. 9(a) that simulated reflection coefficients exhibit operating frequency range from 3.1 to 15.2 GHz (S_{ii} < -10 dB) except for notched bands at 4.7-6 GHz, 6.5-8.1 GHz, 8.56-10.6 GHz, and 11.6-12.9 GHz. As per observation, the maximum peak of S_{ii} (dB) at 8.5 GHz increases by 7 dB for 9-10.6 GHz. The simulated and measured results of S_{ij} (dB) for $i \neq j$ are shown in Figs. 9(b)-(c). As per observation in Fig. 9(b), the simulated and measured mutual coupling is less than -20 dB. Although isolation is greater than 20 dB in the spectrum, the measured result of S_{41} (dB) is ≤ -20 dB and the simulated result is less ≤ -16 dB in the frequency range of 3 to 4.5 GHz. The reduction in magnitude of measured S-

parameters at different frequencies can be attributed to the effects of SMA connector soldering, cables and adapters losses, and the FR4 substrate losses at higher frequencies.

FIGURE 8. Setup of VNA for S-parameters measurement.

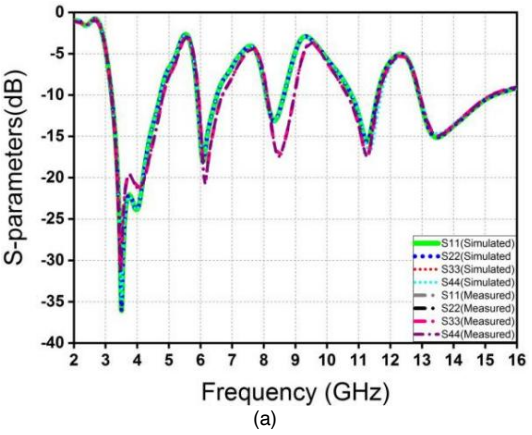

(a)

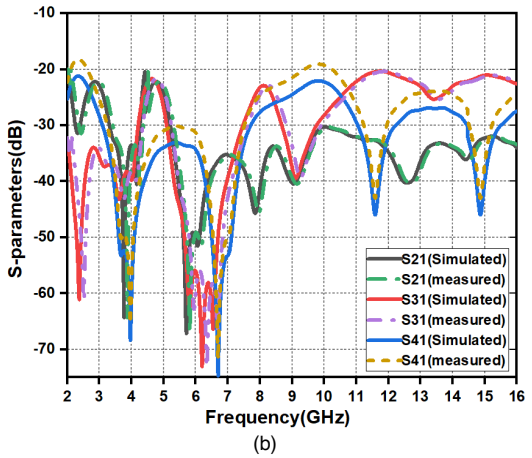

(b)

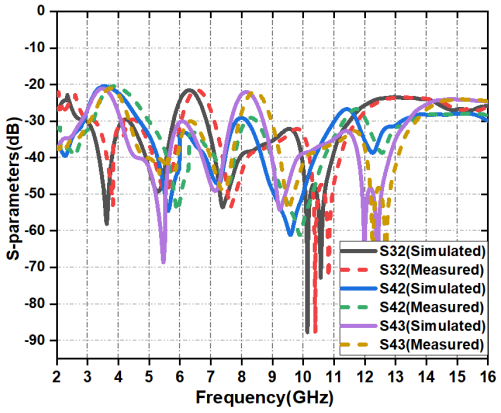

(c)

FIGURE 9. Simulated and measured (a) reflection coefficients (dB), (b) Transmission coefficients/S_{21}, S_{31}, and S_{41} (dB), (c) Transmission coefficients/S_{32}, S_{42}, and S_{43} (dB).

B. FAR-FIELD CHARACTERISTICS

To measure far-field characteristics like 2D radiation patterns (YZ- and XZ-plane) and gain, the fabricated antenna is placed in an anechoic chamber as illustrated in Fig. 10. To understand the complete process of far-field measurement, the setup of RF anechoic chamber is illustrated in Fig. 11. As per observation, the horn antenna is used as a transmitter antenna for transmitting electromagnetic signals throughout far-field measurement and under test fabricated MIMO antenna has been placed on rotatory testing bench, which can move to theta and phi angles for measurement of 2D radiation patterns [19]. For measuring the co-polarization and cross-polarization radiation patterns at each frequency, port 1 is excited, and other ports are terminated with 50 Ω matched loads.

Furthermore, measured and simulated radiation characteristics of the MIMO antenna in the YZ-plane and XZ-plane are compared at various frequencies 3.5 GHz, 8 GHz, and 13 GHz in Figs. 12(a)-(c). As per observation, the cross-polarization is below 15 dB as compared to co-polarization pattern. The simulated and measured radiation patterns are quasi-omnidirectional at $\varphi = 0^{\circ}$ (H-plane) and $\varphi = 90^{\circ}$ (E-plane).The simulated radiation patterns show good agreement with measured radiation patterns at different pass band resonant frequencies. Due to connector losses and cable effects, some slight deviations are observed in measured radiation patterns with simulated patterns.

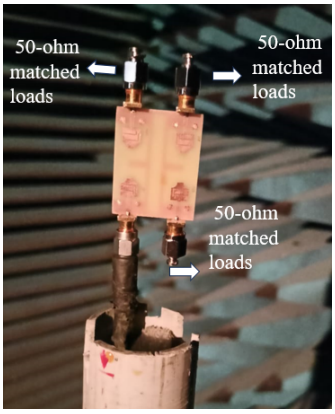

FIGURE 10. Anechoic chamber setup for far-field measurement of the fabricated antenna.

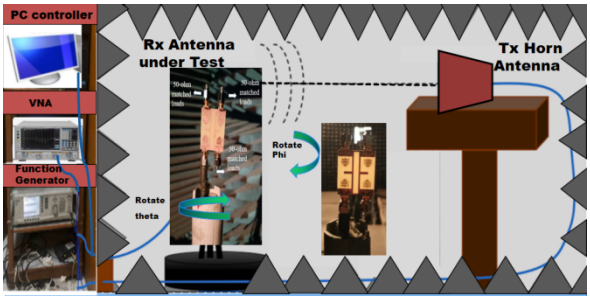

FIGURE 11. Far-field parameters measurement setup in RF anechoic chamber.

The simulated and measured gain values of the proposed UWB MIMO antenna with quad-band rejection capability are illustrated in Fig. 13. As per observation, the values of gain (dB) are negative in rejection bands in the WLAN band, X-band uplink and downlink satellite system, X-band NATO type-2 spectrum, and Ku-band FSS and DBS services. As per observation, the gain range varies from 4 to 5.6 dB in the UWB spectrum except in the notched bands.

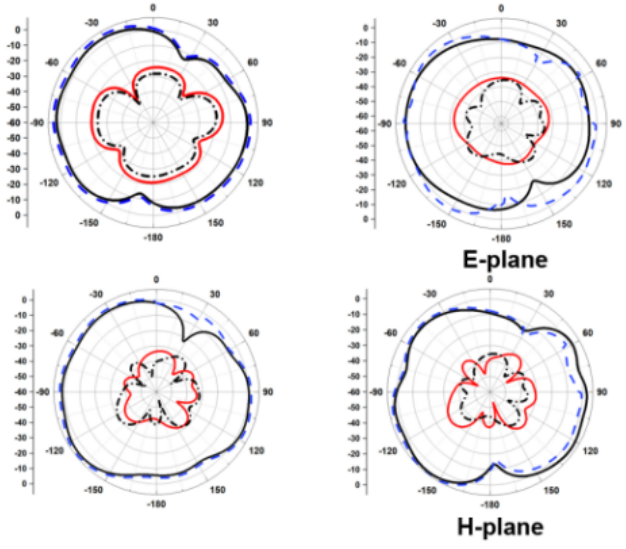

(a) (b)

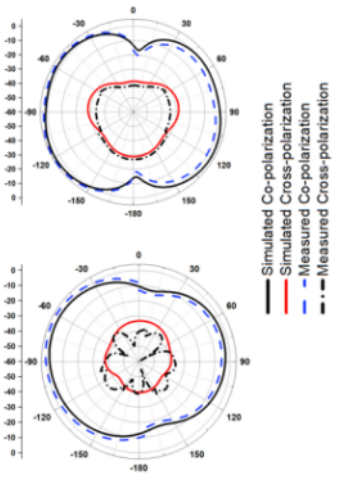

(c)

FIGURE 12. Simulated and measured radiation patterns at (a) 3.5 GHz, (b) 8 GHz, (c) 13 GHz.

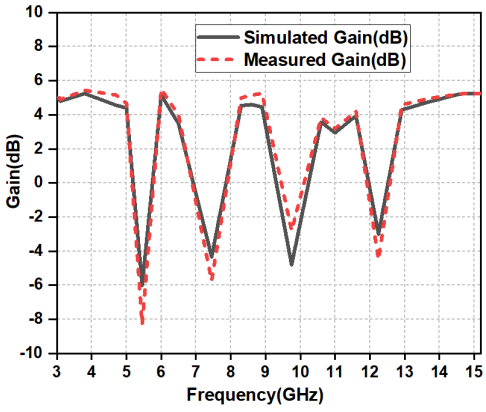

FIGURE 13. Simulated and measured gain (dB) of the antenna.

C. DIVERSITY PERFORMANCE ANALYSIS OF THE PROPOSED MIMO ANTENNA

The correlation among radiating elements is computed by the envelope correlation coefficient (ECC) parameter [24]. According to equation (10), the ECC of the MIMO antenna is a function of S-parameters [35]-[36]. Therefore, the values of ECC are depicted in Fig. 14(a).

$$\rho_{ecc,ij} = \frac{\left[\sum_{n=1}^{N} S_{in}^{*} S_{nj}\right]^{2}}{\left(1-\sum_{n=1}^{N}|S_{ni}|^{2}\right)\left(1-\sum_{n=1}^{N}S_{nj}|^{2}\right)} \quad (10)$$

The simulated and measured values of ECC are <0.001 throughout the spectrum except for rejection bands. The diversity gain (DG) of the proposed antenna is shown in Fig. 14(b). The DG of the proposed antenna between all ports is calculated using equation (11). It can be seen from Fig. 14(b) that the simulated results and measured results of DG are >9.95 dB.

$$DG(dB) = 10 * \sqrt{1 - |ECC|^2} \quad (11)$$

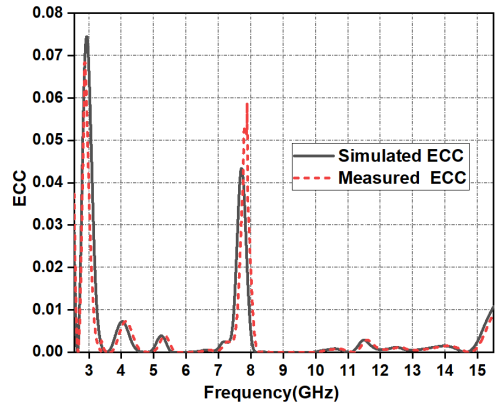

(a)

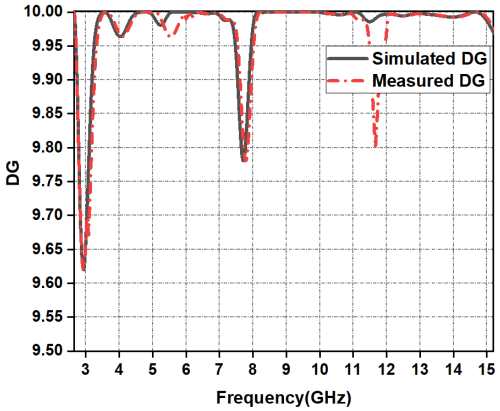

(b)

FIGURE 14. Simulated and measured MIMO characteristics (a) ECC, (b) DG.

Mean effective gain (MEG) is one of the key metrics of a MIMO antenna and can be calculated by equation (12). The simulated results are less than -3 dB throughout the spectrum as shown in Fig. 15.

$$MEG = \int_0^{2\pi}\int_0^{\pi}\left[\frac{XPR}{1+XPR}F_\theta(\theta,\phi)P_\theta(\theta,\phi)+\frac{1}{1+XPR}F_\phi(\theta,\phi)P_\phi(\theta,\phi)\right]\sin\theta d\theta d\phi \quad (12)$$

where F_θ and F_ϕ are the gain behavior of the MIMO elements. Furthermore, MEGs are also calculated in isotropic medium, Laplacian medium, and Gaussian medium at XPR = 0 and 6 dB. In all mediums, the values of MEGs are less than -3 dB, which exhibits satisfactory diversity performance of the proposed MIMO antenna.

For the MIMO system, the ideal value of the total active reflection coefficient (TARC) is below 0 dB. The simulated and measured value of TARC through the spectrum is shown in Fig. 16. It is observed that the TARC is under -10 dB for the proposed antenna. The computations of TARC values is done by equation (13).

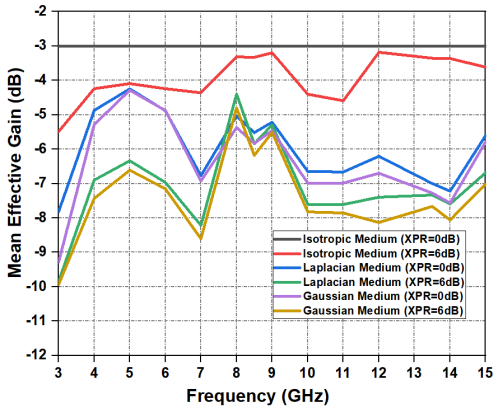

FIGURE 15. Simulated MEG of the proposed MIMO antenna.

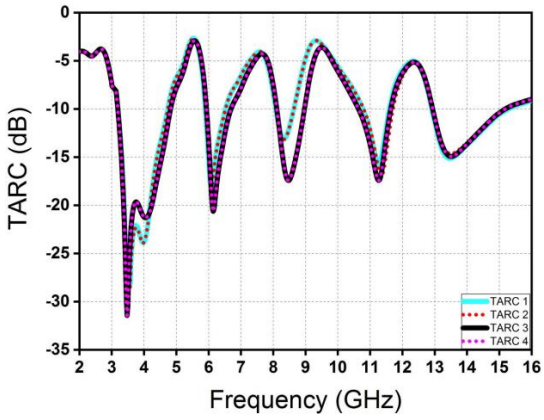

FIGURE 16. Simulated and measured TARC.

$$TARC(dB) = \frac{\sqrt{\sum_{i=1}^{4}\left|S_{ij}+\sum_{n=2}^{4}S_{in}e^{j\theta}n-1\right|^2}}{\sqrt{4}} \quad (13)$$

where range of *i*th port = 1, 2, 3, 4, *n*th port = 2, 3, 4, and θ is the input feeding phase from port.

D. COMPARISON OF PROPOSED MIMO ANTENNA WITH EXISTING ANTENNAS

The comparative analysis of the proposed MIMO antenna with quad-band rejection characteristics is summarized in Table II. The proposed MIMO antenna is compared with existing antennas in terms of size, impedance bandwidth, number of notch bands, number of ports and isolation among them, and gain (dB).

The quad-band notch rejection capability of the proposed antenna is different from existing antennas with single [24, 25], dual [26], [27], and triple notches rejection capability [30]. The proposed MIMO antenna is compared with four port MIMO antenna [24]-[27] and [30].

As per the comparison analysis in Table II, only [22] has discussed dual-port MIMO antenna with quad notches [22], which is larger than four-port MIMO antenna with quad-band rejection characteristics. The proposed MIMO antenna is unique in terms of quad band rejection

characteristics, low size, and stable gain range of 4-5.6 dB. By reducing interference from other sources, the presented band-notched MIMO antenna can enhance the quality of the received signals, leading to better data rates. In the proposed antenna, there is no need for additional filtering components to mitigate interference, which leads to simpler and cost-effective design. The presented MIMO antenna is designed to work across various communication standards, ensuring compatibility and versatility in different applications.

TABLE II. Performance comparison of the proposed antenna with existing antennas reported in the literature.

Ref.	Size (mm^3)	Mutual Coupling (dB)	Port	Notch Bands	Peak Gain (dB)	ECC/DG (dB)
[22]	43×34.9×1.6	-25	2	4	5	<0.01/9.9
[23]	48×34×1.6	-23	4	---	0.95-2.9	<0.039/9.5
[24]	50×50×1.6	<-17	4	1	2.65-5.8	<0.45/---
[25]	47×47×1.6	<-22	4	1	3.5	<0.005/9.98
[26]	73×73×0.79	<-20	4	2	---	<0.0015/9.8
[27]	100×100×1.6	<-20	4	2	---	<0.10/---
[30]	78×78×1.5	<-20	4	3	5.1	<0.05/9.98
Prop.	28×36×1	<-20	4	4	4-5.6	<0.001/9.95

IV. CONCLUSION

A tapered fed quad-port MIMO antenna with quadruple band-notched features is designed and verified with the fabricated prototype. The proposed antenna designed with impedance bandwidth of 3.1-15.2 GHz except for the four notched rejecting interference bands of WLAN (4.7-5.9 GHz), X-band uplink and downlink satellite systems (6.6-8.1GHz), X-band NATO type-2 spectrum (8.6-10.96 GHz), and Ku-band FSS and DBS services (11.6-12.9 GHz), respectively. Furthermore, the proposed antenna achieves mutual coupling of <-20dB. Analysis of diversity performance parameters of designed MIMO antenna are found to be in good agreement with the standard values. Hence, the proposed MIMO antenna with rejection capability has a compact structure with all satisfactory parameters of the diversity antenna.

REFERENCES

[1] Srivastava, K., Kanaujia, B. K., Dwari, S., Kumar, S., & Khan, T. (2019). 3D cuboidal design MIMO/diversity antenna with band-notched characteristics. AEU-International Journal of Electronics and Communications, 108, 141-147.

[2] Sharma, M. K., Kumar, M., Saini, J. P., & Singh, S. P. (2020). Computationally optimized MIMO antenna with improved isolation and extended bandwidth for UWB applications. Arabian Journal for Science and Engineering, 45(3), 1333-1343.

[3] C. King, College Station, Fundamentals of wireless communications. Presented at 2014 67th Annual Conference for Protective Relay Engineers, Texas, (2014).

[4] Weisenhorn, M., & Hirt, W. (2003, May). Performance of binary antipodal signaling over indoor UWB MIMO channel. In IEEE International Conference on Communications, 2003. ICC'03. (Vol. 4, pp. 2872-2878). IEEE.

[5] Marchais, C. L. A. I. R. E., Le Ray, G. I. L. L. E. S., & Sharaiha, A. (2006). Stripline slot antenna for UWB communications. IEEE antennas and wireless propagation letters, 5, 319-322.

[6] FCC, Washington, DC, Federal Communications commission revision of part 15 of the commission's rules regarding ultra-wideband transmission systems. First reported Order FCC: 02.V48, 2002.

[7] Yu, J. F., Liu, X. L., Shi, X. W., & Wang, Z. (2014). A compact four-element UWB MIMO antenna with QSCA implementation. Progress In Electromagnetics Research Letters, 50, 103-109.

[8] Naidu, P. R. T., Saha, C., Krishna, K. V., Shaik, L. A., Siddiqui, J. Y., & Antar, Y. (2020). Compact multiple EBG cells loaded UWB-narrowband antenna pair with high isolation for cognitive radio (CR) based MIMO applications. AEU-International Journal of Electronics and Communications, 127, 153420.

[9] Chacko, B. P., Augustin, G., & Denidni, T. A. (2013). Uniplanar polarisation diversity antenna for ultra-wideband systems. IET Microwaves, Antennas & Propagation, 7(10), 851-857.

[10] Zhao, Y., Zhang, F. S., Cao, L. X., & Li, D. H. (2019). A compact dual band-notched MIMO diversity antenna for UWB wireless applications. Progress In Electromagnetics Research C, 89, 161-169.

[11] Tang, T. C., & Lin, K. H. (2014). An ultrawideband MIMO antenna with dual band-notched function. IEEE Antennas and wireless propagation letters, 13, 1076-1079.

[12] Kang, L., Li, H., Wang, X., & Shi, X. (2015). Compact offset microstrip-fed MIMO antenna for band-notched UWB applications. IEEE antennas and wireless propagation letters, 14, 1754-1757.

[13] Zhang, J., Chen, T., Hua, L., & Wang, W. (2019). A compact differential-fed UWB antenna with band-notched characteristics. Progress In Electromagnetics Research M, 83, 171-179.

[14] Kumar, A., Ansari, A. Q., Kanaujia, B. K., & Kishor, J. (2019). A novel ITI-shaped isolation structure placed between two-port CPW-fed dual-band MIMO antenna for high isolation. AEU-International Journal of Electronics and Communications, 104, 35-43.

[15] Kumar, A., Ansari, A. Q., Kanaujia, B. K., Kishor, J., & Kumar, S. (2020). An ultra-compact two-port UWB-MIMO antenna with dual band-notched characteristics. AEU-International Journal of Electronics and Communications, 114, 152997.

[16] Kapil, M., & Sharma, M. (2019, March). Dual notched band UWB wireless MIMO antenna. In 2019 6th International Conference on Signal Processing and Integrated Networks (SPIN) (pp. 8-12). IEEE.

[17] Gautam, A. K., Yadav, S., & Rambabu, K. (2018). Design of ultra-compact UWB antenna with band-notched characteristics for MIMO applications. IET Microwaves, Antennas & Propagation, 12(12), 1895-1900.

[18] Tang, T. C., & Lin, K. H. (2014). An ultrawideband MIMO antenna with dual band-notched function. IEEE Antennas and wireless propagation letters, 13, 1076-1079.

[19] Jaglan, N., Kanaujia, B. K., Gupta, S. D., & Srivastava, S. (2018). Design of band-notched antenna with DG-CEBG. International Journal of Electronics, 105(1), 58-72.

[20] Zhang, Y., Jiao, Y. C., Yang, M. M., & Zhao, B. L. (2019, October). A tri-band notched Ultra-wideband MIMO Antenna. In 2019 International Symposium on Antennas and Propagation (ISAP) (pp. 1-3). IEEE.

[21] Agarwal, M., Dhanoa, J. K., & Khandelwal, M. K. (2020). Ultrawide band two-port MIMO diversity antenna with triple notch bands, stable gain and suppressed mutual coupling. AEU-International Journal of Electronics and Communications, 120, 153225.

[22] Modak, S., & Khan, T. (2021). A slotted UWB-MIMO antenna with quadruple band-notch characteristics using mushroom EBG structure. AEU-International Journal of Electronics and Communications, 134, 153673.

[23] Tiwari, R. N., Singh, P., Kanaujia, B. K., & Srivastava, K. (2019). Neutralization technique based two and four port high isolation MIMO antennas for UWB communication. AEU-International Journal of Electronics and Communications, 110, 152828.

[24] Khan, M. S., Naqvi, S. A., Iftikhar, A., Asif, S. M., Fida, A., & Shubair, R. M. (2020). A WLAN band-notched compact four element UWB MIMO antenna. International Journal of RF and Microwave Computer-Aided Engineering, 30(9), e22282.

[25] Ibrahim, A. A., & Abo Sree, M. F. (2022). UWB MIMO antenna with 4-element, compact size, high isolation and single band rejection for high-speed wireless networks. Wireless Networks, 28(7), 3143-3155.

[26] Eltrass, A. S., & Elborae, N. A. (2019). New design of UWB-MIMO antenna with enhanced isolation and dual-band rejection for WiMAX and WLAN systems. IET Microwaves, Antennas & Propagation, 13(5), 683-691.

[27] Shehata, M., Said, M. S., & Mostafa, H. (2018). Dual notched band quad-element MIMO antenna with multitone interference suppression for IR-UWB wireless applications. IEEE Transactions on Antennas and Propagation, 66(11), 5737-5746.

[28] Chen, Z., Zhou, W., & Hong, J. (2021). A miniaturized MIMO antenna with triple band-notched characteristics for UWB applications. IEEE access, 9, 63646-63655.

[29] Jayant, S., & Srivastava, G. (2022). Close-Packed quad-element triple-band-notched UWB MIMO antenna With upgrading capability. IEEE Transactions on Antennas and Propagation, 71(1), 353-360.

[30] El-Gendy, M. S., Ali, M. M. M., Thompson, E. B., & Ashraf, I. (2023). Triple-Band Notched Ultra-Wideband Microstrip MIMO Antenna with Bluetooth Band. Sensors, 23(9), 4475.

[31] Dong, Y. D., Hong, W., Kuai, Z. Q., & Chen, J. X. (2009). Analysis of planar ultrawideband antennas with on-ground slot band-notched structures. IEEE Transactions on Antennas and Propagation, 57(7), 1886-1893.